Cerebral Cortex, November 2018;28: 4105–4119

doi: 10.1093/cercor/bhy225
Advance Access Publication Date: 12 September 2018
Original Article

ORIGINAL ARTICLE

Inhibitory Neuron Activity Contributions to Hemodynamic Responses and Metabolic Load Examined Using an Inhibitory Optogenetic Mouse Model

Alberto L. Vazquez[1,2], Mitsuhiro Fukuda[1] and Seong-Gi Kim[3,4]

[1]Department of Radiology, University of Pittsburgh, Pittsburgh, PA 15213, USA, [2]Department of Bioengineering, University of Pittsburgh, Pittsburgh, PA 15203, USA, [3]Department of Biomedical Engineering, Sungkyunkwan University, Suwon, Korea and [4]Center for Neuroscience Imaging Research, Institute for Basic Science, Sungkyunkwan University, Suwon, Korea

Address correspondence to Alberto L. Vazquez, 3025 E Carson St., McGowan Institute, Rm 159, Pittsburgh, PA 15203, USA. Email: alv15@pitt.edu

Abstract

Hemodynamic signals are routinely used to noninvasively assess brain function in humans and animals. This work examined the contribution of inhibitory neuron activity on hemodynamic responses captured by changes in blood flow, volume and oxygenation in the cortex of lightly anesthetized mice. Because cortical activity is not commonly initiated by inhibitory neurons, experiments were conducted to examine the neuronal activity properties elicited by photo-stimulation. We observed comparable increases in neuronal activity evoked by forelimb and photo-stimulation; however, significantly larger increases in blood flow and volume were produced by photo-stimulation of inhibitory neurons compared with forelimb stimulation. Following blockade of glutamate and GABA-A receptors to reduce postsynaptic activity contributions, neuronal activity was reliably modulated and hemodynamic changes persisted, though slightly reduced. More importantly, photo-stimulation-evoked changes in blood flow and volume were suppressed by 75–80% with the administration of a nitric oxide synthase inhibitor, suggesting that inhibitory neurons regulate blood flow mostly via nitric oxide. Lastly, forelimb and photo-stimulation of excitatory neurons produced local decreases in blood oxygenation, while large increases were generated by photo-stimulation of inhibitory neurons. Estimates of oxygen metabolism suggest that inhibitory neuron activity has a small impact on tissue metabolic load, indicating a mismatch between the metabolic demand and blood flow regulation properties of inhibitory and excitatory neurons.

Key words: excitation, fMRI, inhibition, metabolism, optogenetics

Introduction

Hemodynamic methods to image brain function are indirectly sensitive to neuronal activity due to their vascular nature, limiting their interpretability and quantification. Widely used methods like blood-oxygenation level dependent functional magnetic resonance imaging (BOLD fMRI) are further complicated by their opposite sensitivity to cerebral blood flow (CBF), and cerebral blood volume (CBV) and cerebral oxidative

metabolism (Buxton et al. 1998; Davis et al. 1998; Kim et al. 1999). Although significant progress has been achieved in determining the properties of hemodynamic responses (Kida and Hyder 2006; Hillman 2014), fundamental questions remain uncertain. For instance, the relative contribution of excitatory and inhibitory neuron activity to hemodynamic responses and metabolic load is unclear. Increases in neuronal activity in cortex are largely excitatory (e.g., visual or somatosensory stimulation) and generally produce increases in CBF and the cerebral metabolic rate of oxygen metabolism (CMR_{O2}); however, the impact of increases in inhibitory neuron activity on vascular and metabolic responses is less clear. Arguments for increases and decreases (often termed deactivation) in hemodynamic signals have been proposed with increases in inhibitory activity (Stefanovic et al. 2004; Shmuel et al. 2006; Devor et al. 2008; Boorman et al. 2015). Successfully delineating the contributions of excitatory and inhibitory activity to neurovascular and neurometabolic coupling is an important and necessary step towards understanding hemodynamic signals as well as their sensitivity to brain function and dysfunction at the neuronal level. In particular, inhibitory neuron dysfunction has been implicated in several neurological and psychiatric disorders including epilepsy and schizophrenia (Sloviter 1987; Lewis et al. 2005).

Inhibitory neurons are less numerous than excitatory neurons in cortex, consisting of about 10–20% of all neurons, but they play a critical role in cortical processing. They rely on γ-aminobutyric acid (GABA) neurotransmission to inhibit the activity of postsynaptic neurons that can be excitatory or inhibitory. In cortex, their connections are mostly local and remain within the same region (Taniguchi 2014). Some inhibitory neurons extend projections to nearby arterial vasculature, potentially making them important players in neurovascular regulation (Cauli 2004; Cauli and Hamel 2010; Perrenoud et al. 2012). More importantly, subpopulations of inhibitory neurons release nitric oxide (Taniguchi 2014), a potent vasodilator, which could serve as a principal mediator of changes in blood flow. The role of inhibitory neuron activity on vascular and metabolic responses can be investigated in the living brain using targeted optogenetic approaches. Using an optogenetic mouse model that expresses channelrhodopsin-2 (ChR2) in cortical inhibitory neurons, 2 independent reports by Anenberg et al. and Uhrilova et al. showed that photo-stimulation of inhibitory neurons produces significant increases in blood flow and arterial diameter (Anenberg et al. 2015; Uhlirova et al. 2016). In addition, Anenberg et al. (2015) showed that under pharmacological blockade of glutamate receptors, optogenetically driven increases in blood flow remained. Uhrilova et al. (2016) showed that a typical poststimulation undershoot following the increase in arterial diameter was mitigated with the administration of a neuropeptide-Y (NPY) receptor antagonist. In summary, these results demonstrate inhibitory neurons play a very significant role in generating hemodynamic responses. However, relevant signaling pathways underlying these changes in blood flow and the impact of inhibitory neuron activity on tissue metabolism remain unresolved.

We sought to use this optogenetic model targeting the vesicular GABA transporter (VGAT) to compare vascular and metabolic responses evoked by inhibitory neuron activity to that of largely excitatory activity produced by sensory activity. The goals of this work are: 1) Determine the relationship between inhibitory neuronal activity and the hemodynamic response (e.g., are the evoked hemodynamic responses from forelimb stimulation and initial inhibitory activity similar? Is the hemodynamic response elicited by inhibitory activity dependent on the evoked spiking activity or LFP activity?). 2) Determine whether inhibitory-driven changes in blood flow are mediated by nitric oxide. 3) Is the metabolic load of excitatory neuron activity similar to that of inhibitory neuron activity? Are the changes in CBF proportional to the metabolic changes? For this last goal, experiments were also performed in an optogenetic mouse model targeting cortical excitatory neurons.

Neurovascular and neurometabolic responses were investigated by simultaneously recording field potential (FP) and multiunit activity (MUA) using a metal electrode, blood flow using laser Doppler flowmetry (LDF), and blood volume-sensitive and blood oxygenation-sensitive responses using optical imaging of intrinsic signal (OIS). The intensity and duration of photostimuli were varied to modulate the activity of the targeted area, the forelimb region in the somatosensory cortex. We performed initial experiments to ensure that evoking activity in inhibitory neurons by photo-stimulation can produce graded levels of activity without generating aberrant activity patterns or activity that exceeds that from forelimb stimulation. To this end, we compared electrophysiological responses to photostimulation and forelimb stimulation with cortical depth. Ensuing experiments were performed under 3 pharmacological conditions (Fig. 1) while recording hemodynamic responses and electrophysiology at a single depth location. These pharmacological experiments were designed to ensure excitatory neuron activity is not being modulated by disinhibition (Fig. 1*B*, Condition 1), minimize the influence of GABA neuron activity on postsynaptic neurons (Fig. 1*B*, Conditions 1 and 2), and determine the impact of NO signaling on hemodynamic responses (Fig. 1*B*, Condition 3). Blockade of glutamate receptors (Conditions 1 and 2) prevent the propagation of excitatory activity, which may occur by inhibiting the inhibitory drive of excitatory neurons with photo-stimulation of inhibitory neurons. Under this condition, the blockade of GABA receptors is also possible without enhancing neuronal activity.

Materials and Methods

General Preparation

A total of 22 adult transgenic mice (strain B6.Cg-Tg(Slc32a1-COP4*H134R/eYFP)8Gfng/J; 23–32 g; 2–7 months old) expressing ChR2 in inhibitory neurons targeted via the VGAT (Zhao et al. 2011) were obtained from the Jackson Laboratory (Bar Harbor, ME). All procedures performed followed an experimental protocol approved by the University of Pittsburgh Institutional Animal Care and Use Committee in accordance with the standards for humane animal care and use as set by the Animal Welfare Act and the National Institutes of Health Guide for the Care and Use of Laboratory Animals. Mice were initially anesthetized using a ketamine (75 mg/kg) and xylazine (10 mg/kg) or dex-dormitor (0.5 mg/kg) cocktail administered intraperitoneally (IP). An IP line was then inserted to administer fluids (5% dextrose in saline) as well as supplementary anesthesia throughout the experiment, which consisted of ketamine alone at 30 mg/kg/h, typically commencing about 1 h after induction. Two needle electrodes were placed in the left forepaw between digits 2 and 4 for electrical stimulation. The animals were then placed in a stereotaxic frame (Narishige, Tokyo, Japan) and supplementary oxygen was administered blow-by using a cannula at a rate of 500 mL/min. Body temperature was maintained at 37 °C and heart rate was continuously monitored throughout the experiment as described previously to assess the physiological condition of the animal and depth of anesthesia. Surgery

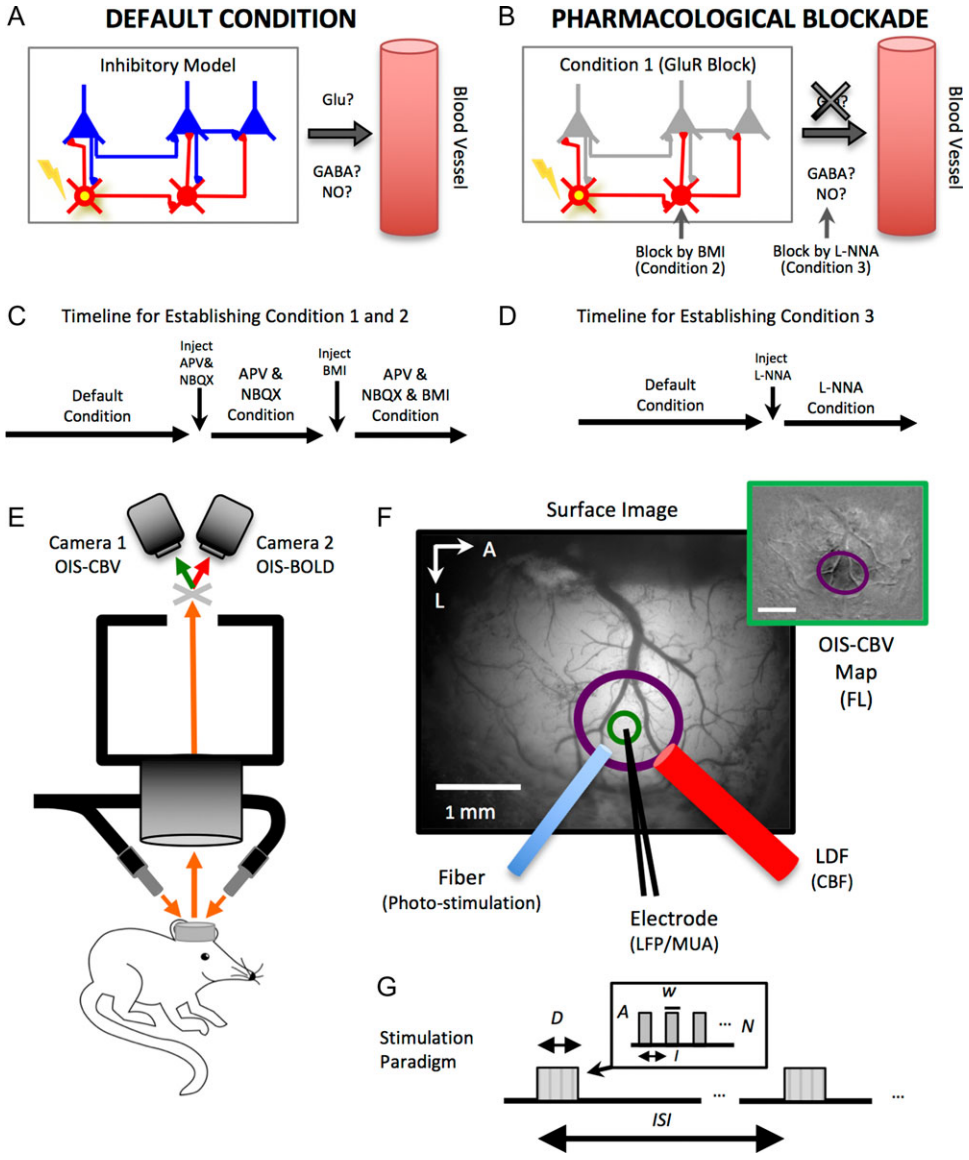

Figure 1. Simplified schematic of the experimental conditions implemented in this work and experimental setup. (*A*) Under default conditions (light ketamine anesthesia), photo-stimulation activates inhibitory neurons (yellow soma) which will likely inhibit postsynaptic excitatory (glutamatergic in blue) and inhibitory (gabaergic in red) neurons. Some inhibitory neurons are known to release nitric oxide (NO), a potent vasodilator. (*B*) Experiments were also performed under pharmacological blockade of glutamate receptor (GluR) activity to prevent the modulation of excitatory activity (Condition 1). Pharmacological blockade of $GABA_A$ receptors was also used to prevent fast inhibitory action on inhibitory (and excitatory) neurons (Condition 2). Lastly, experiments were performed under pharmacological blockade of nitric oxide synthase (NOS) to determine the role nitric oxide on blood flow regulation by inhibitory neuron activity (Condition 3). (*C*) Timeline for establishing Conditions 1 and 2. These conditions were established in sequence. Experiments under a combination of APV, NBQX, and BMI were conducted while monitoring background ongoing activity to ensure this condition is maintained during data collection. (*D*) Timeline for establishing Condition 3. Experimental setup. (*E*) Optical images of intrinsic signal (OIS) were acquired simultaneously from the somatosensory cortex of lightly anesthetized mice using a dual camera system. One camera acquired images sensitive to changes in cerebral blood volume (OIS–CBV) and the other camera acquired images sensitive to changes in blood oxygenation (OIS–BOLD). The brain was illuminated with orange light and appropriately filtered prior to each camera. (*F*) Probe placement and ROI. An initial mapping experiment was used to map the location of the forelimb somatosensory cortex for further experimentation (top-right inset; scale bar = 1 mm). The optic fiber, electrode, and laser Doppler flowmetry (LDF) probe were placed in the center of the activated region (purple circle) while avoiding large surface vasculature. The ROI used to obtain OIS time series (OIS–CBV and OIS–BOLD) is shown in green, it excluded surface vasculature. (*G*) Stimulation paradigm. Forelimb or photo-stimuli were delivered with amplitude *A*, pulse duration *w*, at a frequency or interval *I*, over an overall stimulus duration *D*. These stimulation trials were repeated after time period ISI.

consisted of removing the skin and exposing the skull parietal bone over the somatosensory area to make a cranial window. A well was made using acrylic cement surrounding an area about $4 \times 3\,mm^2$, centered about 2 mm lateral and 1 mm rostral from Bregma. The skull was then removed using a dental drill and cerebrospinal fluid was released around the cisterna magna area to minimize edema. Surgical light exposure to the brain during and after the craniotomy was filtered to green–yellow light (570 ± 10 nm) to avoid exposure to white light, which could continuously stimulate the exposed brain tissue. The well area was then filled with 1% agarose gel at body temperature.

Imaging Setup and Probe Placement

The location of the forelimb area was then identified for electrode and probe placement using CBV weighted OIS (OIS–CBV) at a wavelength of 572 nm (Fig. 1*E*). This wavelength corresponds to an isosbestic point for hemoglobin, making the OIS data sensitive to changes in the total amount of hemoglobin and therefore representative of CBV (Horecker 1943). Follow-up experiments also acquired optical imaging signals at a wavelength of 620 nm, sensitive to blood deoxy-hemoglobin and therefore the blood oxygenation level (OIS–BOLD) (Horecker 1943). These data allowed us to examine potential differences in oxidative metabolism responses. To serve both purposes, a dual-camera system (Dual-cam, Photometrics Inc., Tucson, AZ, USA) was used to capture OIS–CBV and OIS–BOLD images simultaneously when necessary. OIS–CBV and OIS–BOLD data were acquired at 30 frames per second (fps) using analog CCD cameras (Sony XT-75, Japan) and an A/D frame-grabbing board (Matrox, Inc., Dorval, Quebec) over a field-of-view of 4.4 × 3.7 to 3.5 × 3.0 mm^2 depending on the magnification setting of the macroscope (MVX-10; Olympus, Tokyo, Japan; Fig. 1*E*). The brain was illuminated using oblique light guides connected to a halogen light source (Thermo-Oriel, Stratford, CT, USA) to transmit filtered light at a wavelength of 600 ± 50 nm. A 572 ± 7 nm barrier filter was placed prior to the OIS–CBV camera and a 620 ± 7 nm barrier filter was placed prior to the OIS–BOLD camera to obtain the desired sensitivities.

For the initial mapping experiment, the forelimb stimulus consisted of 1.2 mA, 0.5 ms electrical pulses at a frequency of 5 Hz for 3 s every 16 s, repeated 10 times. The stimulus was delivered using a current isolator box (AMPI, Jerusalem, Israel) driven by a Master-9 waveform generator (AMPI, Jerusalem, Israel). Forelimb activity maps were generated by computing an average difference image of the data obtained over each stimulation trial and the data from each 2 s period preceding stimulation onset (–3 to –1 s).

An optic fiber, metal electrode and LDF probe were placed as close as possible to the OIS–CBV hotspot location while avoiding large surface vessels (Fig. 1*F*). The optic fiber used to deliver the photo-stimulus has a core diameter of 125 μm (S-405-HP, ThorLabs, Inc., Newton, NJ). The metal electrode (Carbostar-1 with tip diameter of 5 μm and resistance of about 1 MΩ; Kation Scientific, Minneapolis, MN) was placed adjacent to the optic fiber below the core of the illuminated area at a depth of 260 μm. Lastly, the LDF (Perimed Inc., Jarfalla, Sweden) probe used has a tip diameter of 450 μm and operating wavelength of 780 nm. It was placed over the area illuminated by the optic fiber and the location of the metal electrode to monitor and record CBF. Because each probe was placed under the optical imaging system, the fiber, electrode, and probe were inserted at a 60° angle. The location of the optic fiber and LDF probe was fixed throughout the experiments. Recording depths are reported relative to a vertical axis to account for the angled insertion.

Experimental Design

Photo-stimulation and forelimb stimulation experiments were targeted for all animals. The photo-stimulus was delivered using a power-adjustable, TTL-controlled, 473 nm laser diode unit (CrystaLaser, Inc., Reno, NV) connected to the optic fiber. The photo-stimulus pulse duration was varied to modulate the spike rate in the stimulated area. Preliminary experiments designed to evoke activity within physiological ranges suggested that a pulse amplitude (*A* in Fig. 1*G*) of 1 mW and pulse durations (*w* in Fig. 1*G*) of 30, 10, and 2 ms are suitable to elicit high and low spike rates. Since these parameters were also used in previous studies from our group using an excitatory optogenetic mouse model (Vazquez et al. 2014), we selected them for further experimentation in this model. For comparison, responses obtained by forelimb stimulation using 1.2 mA and 0.5 ms pulses were also recorded. Although these 2 modes of activation recruit activity from different neuronal populations (at least initially), it allowed us to evaluate our photo-stimulation parameters to ensure that they did not produce aberrant activity patterns or spike rates larger than those of sensory stimulation.

Five experimental sessions were performed to address the aims of this work. Experiment 1 examined the neural properties of photo-stimuli. Experiments 2 and 3 investigated the hemodynamic properties of inhibitory neuron activity. Experiment 4 investigated the role of nitric oxide on hemodynamic responses evoked by inhibitory neuron activity. Experiment 5 compared the impact of excitatory and inhibitory activity on oxidative metabolism. Electrophysiological activity was recorded at a frequency of 20 kHz (MAP Data Acquisition System, Plexon, Inc., Dallas, TX). OIS was recorded at 30 fps and LDF was recorded at 1 kHz (MP150, Biopac Systems Inc., Goleta, CA). The total number of animals used for each experimental session is indicated in Table 1.

Experiment 1: Electrophysiological assessment of the evoked photo-stimulation and forelimb stimulation responses as a function of depth. A single pulse was delivered every 3 s for 48 s for each parameter set. In addition to the stimulation parameters described above, experiments were also performed using photo-stimuli with amplitude of 0.25 mW and duration of 30, 10, and 2 ms. Measurements were performed at linear depth increments of 100 μm, which consisted of steps of about 86 μm in the depth direction. Each time the electrode was advanced 100 μm, a few minutes elapsed before recording continued to allow for the electrode to settle. This experiment was performed on 4 animals to examine the neural activity properties of photo-stimulation in this mouse model (VGAT-ChR2).

Experiment 2: Hemodynamic and neural recording of photo-stimulation and forelimb-stimulation responses. LDF, OIS–CBV, OIS–BOLD, FP, and MUA were recorded simultaneously. To evoke robust hemodynamic responses, each recording session consisted of stimulation for 4 s at a frequency of 5 Hz every 60 s repeated 5 times (Fig. 1*G*). A total of at least 10 trials were targeted for each stimulation parameter set. Photo-stimuli were delivered at an amplitude of 1 mW. This experiment was performed in a total of 22 animals, including those animals that participated in Experiments 1, 3, and 4.

Experiment 3: Pharmacological blockade of Glutamate and $GABA_A$ receptors to determine the impact of restricted inhibitory neuron activity on evoked hemodynamic responses. The same experimental and data acquisition strategy as Experiment 2 was followed for these experiments to evoke robust hemodynamic responses. A control data set was acquired under the default

Table 1 Number of animals for each experimental group

Stimulation	Exp. 1	Exp. 2	Exp. 3	Exp. 4	Exp. 5
FL	4	13	8	4	7
1 mW 30 ms (5 Hz)	4	20	8	4	7
1 mW 10 ms (5 Hz)	4	20	8	4	7
1 mW 2 ms (5 Hz)	4	19	8	4	7

physiological condition (light ketamine anesthesia; Condition 1, Fig. 1A). Then, a solution containing the NMDA receptor antagonist DL-2-amino-5-phosphonopentanoic acid (APV, 5 mM; Sigma-Aldrich, Inc.) and the AMPA and kainate receptor antagonist 2,3-dioxo-6-nitro-1,2,3,4-tetrahydrobenzo[*f*]quinoxaline-7-sulfonamide disodium salt (NBQX, 0.5 mM; Tocris Bioscience, Inc.) was administered intracortically by pipette and pressure injection to block glutamate receptors (Condition 1, APV+NBQX; Fig. 1B,C). A small amount of sulforhodamine-101 (SR-101, 10 μM) was used to verify the delivery of agent. A few minutes after the stabilization of electrophysiological activity, experimental recording was repeated. This procedure took about 30 min. Then, the same intracortical injection procedure was used to administer bicuculline methiodide (BMI, 0.5 mM; Sigma-Aldrich, Inc.), a $GABA_A$ receptor antagonist. Experimental recording was repeated again 5–10 minutes after BMI injection (Condition 2, APV+NBQX+BMI; Fig. 1B,C). All solutions were dissolved in 1× PBS (Sigma-Aldrich, Inc.). At least 5 trials were targeted for each stimulation parameter set under default, APV+NBQX and APV+NBQX+BMI conditions. We did not observe unrestricted or aberrant neuronal activity following the administrations of these agents. The APV+NBQX experiment was performed in 7 animals, while the APV+NBQX+BMI experiment was performed in 6 animals.

Experiment 4: Pharmacological blockade of nitric oxide synthase (NOS) to determine the impact of nitric oxide on evoked hemodynamic responses. The same experimental and data acquisition strategy as Experiment 3 was followed for these experiments. The nonselective NOS antagonist Nω-nitro-L-arginine (L-NNA, 0.5 mM; Sigma-Aldrich, Inc.) was administered intracortically to block NOS enzyme activity (Condition 3, Fig. 1B,D). At least 5 trials were targeted for each stimulation parameter set under default and L-NNA conditions. This experiment was performed in 4 animals.

Experiment 5: Hemodynamic changes recorded from Thy1-ChR2 mice were used to compare metabolic load differences between optogenetic responses initiated from excitatory and inhibitory neurons. We acquired OIS–BOLD data from Thy1-ChR2 mice used in a previous study using the same photostimulation parameters as those in Experiments 2–4. These mice express ChR2 in Layer 5 pyramidal neurons and their activation produced activity that propagated throughout the cortex as expected. Refer to (Vazquez et al. 2014) for additional details. Data using this excitatory optogenetic mouse model were acquired from 7 animals.

Data Analysis

All data were analyzed using Matlab (Mathworks, Natick, MA, USA). The electrophysiological data were filtered between 300 and 9000 Hz to quantify MUA and between 10 and 150 Hz to quantify FP activity. MUA was quantified over 50 ms temporal bins by counting the number of outward zero-crossings exceeding a threshold of 3× the standard deviation of prestimulation baseline data. FP was quantified by measuring the magnitude between the peak of the first negative and positive deflections (N1 and P1) as an indication of the event's FP amplitude. Photostimulation was not observed to introduce noise or artifacts into the FP and MUA data; however, electrical forelimb stimulation did introduce a short, high-frequency deflection into data, such that the forelimb electrophysiological data surrounding stimulation onset between −1 and 4 ms were discarded. The MUA and FP data were averaged for each stimulation parameter set for each animal.

Time series of the hemodynamic responses evoked by forelimb and photo-stimulation were obtained from the LDF, OIS–CBV, and OIS–BOLD data. To extract the OIS–CBV and OIS–BOLD time series, a circular ROI 200 μm in diameter was generated at the center of the insertion point of the metal electrode and surface vasculature were excluded from the ROI. LDF, OIS–CBV, and OIS–BOLD time series spanning 60 s were obtained from all trials starting at 5 s prior to stimulation onset. Small linear trends were removed from each trial by considering only data over the first and last 5 s of each time series. To minimize the contribution of YFP emission during the photo-stimulation period to the hemodynamic OIS–CBV and OIS–BOLD time series, the temporal difference was computed for each trial over the prestimulation baseline and stimulation period. Then, data points during the stimulation period exceeding a threshold of > 3× the baseline standard deviation were removed from the time series. The LDF, OIS–CBV and OIS–BOLD time series were down-sampled to 10 Hz and low-pass filtered with a rectangular cut-off of 4 Hz. Lastly, time series from trials with common stimulation parameters were averaged and then normalized by their prestimulation baseline intensity.

The LDF and OIS–CBV change was measured from the average time series as the average value 4–7 s after stimulation onset. The time-to-peak was also measured directly from the time series. We report average values ± standard deviation when available, while the error bars in the figures denote the standard error. Statistical significance was assessed using a *t*-test to determine population differences with respect to prestimulation baseline or responses evoked by other stimuli.

The cerebral metabolic rate of oxygen consumption (CMR_{O2}) was estimated using the average LDF, OIS–CBV, and OIS–BOLD data and the methods described by Dunn et al. (2005). This metric was used to determine differences in metabolic load between the different stimuli used in excitatory and inhibitory optogenetic mouse models. Briefly, changes in oxygenated and deoxygenated hemoglobin (ΔHbO and ΔHbR, respectively) were calculated by decomposition of the OIS data and assuming a resting hemoglobin concentration and oxygen saturation of 100 μM and 60%, respectively (Jones et al. 2001; Dunn et al. 2005). Total hemoglobin was estimated as the summation of oxygenated and deoxygenated hemoglobin (i.e., ΔHbT = ΔHbO + ΔHbR). Changes relative to baseline were calculated using Equation 1 which stems from Fick's law (denoted by "r"; e.g., $rCMR_{O2} = 1 + \Delta CMR_{O2}/CMR_{O2,0}$). Assumptions underlying this steady-state expression is that oxygen delivered to tissue is immediately metabolized and that arterial blood is fully oxygenated. The change in CMR_{O2} was extracted from the calculated $rCMR_{O2}$ time series between 4 and 7 s after stimulation onset.

$$rCMR_{O2} = rCBF\left(\frac{rHbR}{rHbT}\right) \quad (1)$$

Results

All animals underwent an initial experiment to map the location of the forelimb region in the somatosensory cortex. OIS–CBV was used for this purpose where increases in CBV manifest as an increase in light absorption and a darkening of active region (Fig. 1F). The electrode was placed in this region at a depth of 260 μm and the fiber optic and LDF probe were placed over the pial surface away from large vasculature facing the electrode location. Expression of ChR2 was verified by two-

photon microscopy in a subset of animals as evidenced by the fluorescence of YFP along cell membranes (Fig. 2A). Inspection of YFP fluorescence from cell processes and somata was observed along depth at the imaged locations, in agreement with previous reports (Zhao et al. 2011; Uhlirova et al. 2016).

Electrophysiology of Photo-stimulation Versus Forelimb Stimulation in the Somatosensory Cortex as a Function of Depth (Experiment 1)

Single-pulse experiments were performed to characterize the properties of the evoked neuronal activity as a function of cortical depth and compare it to that of sensory forelimb simulation. As expected, forelimb stimulation evoked activity first in Layer 4 (433 μm deep) with the first spike detected on average 9.1 ± 1.6 ms after stimulation onset (Fig. 2B, black line). Forelimb activity quickly propagated up to Layers 2–3 and down to Layer 5 within 1 ms, and was lastly detected deep in Layer 6 on average 14.5 ms after stimulus onset. These data agree with previous studies in mice considering the variability of the responses (Armstrong-James et al. 1992; Vazquez et al. 2014). Photo-stimulation consistently evoked activity first in the most superficial layer sampled (86 μm deep). The average time-to-first spike was measured to be 1.4 ± 1.7 ms, 1.6 ± 1.7 ms, and 1.3 ± 1.2 ms for 1 mW photo-stimuli with duration of 30, 10, and 2 ms, respectively (Fig. 2B, blue, red, and green lines). Activity was evoked progressively later in deeper cortical locations reaching deep Layer 6 on average 5.8 ± 2.5 ms, 5.4 ± 1.8 ms, and 5.2 ± 1.6 ms after 30, 10, and 2 ms photo-stimulus onset (1 mW), respectively. The increase in spike latency with depth is likely due to decreasing light intensities with depth requiring longer to recruit sufficient photo-detectors to evoke activity. Similarly, decreasing the photo-stimulus intensity to 0.25 mW increased the average time-to-first spike by 2.7 ms (Fig. 2B, dashed-red line). The same trend was observed with photo-stimulus intensity in an optogenetic mouse model targeting excitatory neurons (Vazquez et al. 2014).

Ongoing spiking activity was highest in layer 5, as expected for this cortical region (data not shown). Significant increases in spike rate as a function of depth were observed for both forelimb stimulation and all photo-stimuli tested (Fig. 2C). In general, the change in spike rate decreased deeper in the cortex with the shortest photo-stimulus evoking an average spike rate of 1.0 ± 0.2 spikes/s in the deepest sampled location (Fig. 2C, green line). The spike rate at this depth was not significantly different for longer, lower intensity photo-stimulation (1.1 ± 0.2 spikes/s for 0.25 mW, 10 ms), but spikes were not consistently evoked for short duration, lower intensity photo-stimuli (0.3 ± 0.3 spikes/s for 0.25 mW, 2 ms). Altogether, the average increase in spiking activity across all depths was effectively modulated by the photo-stimulation amplitude and duration and the increase in activity did not exceed that of forelimb stimulation

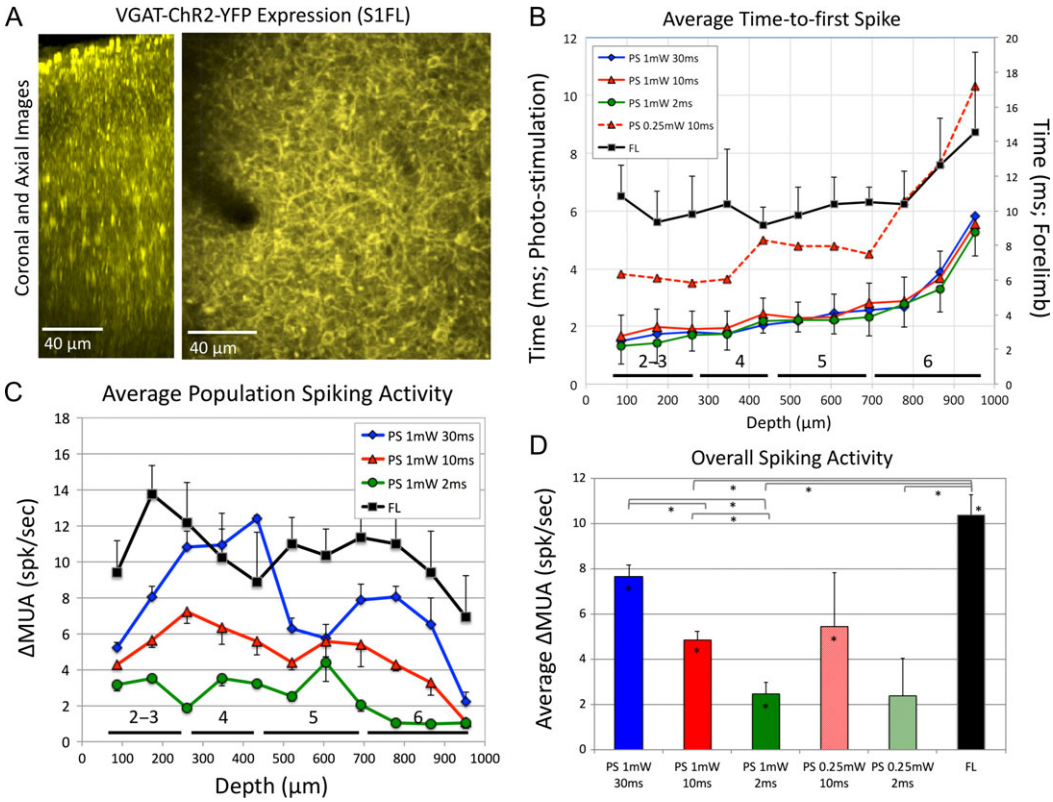

Figure 2. Characterization of the optogenetic inhibitory mouse model. (A) Two-photon microscopy images of ChR2-YFP expression in the somatosensory cortex. Images of an orthogonal section along depth (coronal section on the left) and axial section 200 μm under the cortical surface show the numerous cells expressing ChR2 in the somatosensory cortex. (B) Average time-to-first spike after evoked photo-stimulation (left y-axis) for different stimulation parameters and after forelimb stimulation (black line, right y-axis) as a function of depth. The approximate locations of the cortical layers are shown along the bottom of the horizontal axis (Altamura et al. 2007). (C) Average change in multiunit activity (ΔMUA) as a function of depth for different photo-stimulation parameters as well as forelimb stimulation (black line). (D) Average overall spiking activity for all photo-stimulation parameters tested. On average, forelimb activity was largest though not significantly larger than that evoked by 1 mW 30 ms photo-stimulation. Error bars denote the standard error and statistically significant differences ($P < 0.05$) are denoted by the asterisk in the bar (significantly greater than 0) or the lines above the bar graph for population comparisons.

(Fig. 2D). The average activity evoked by the strongest photo-stimulus was significantly higher than those of shorter pulse durations ($P < 0.05$) and was not significantly different from that evoked by forelimb stimulation ($P > 0.15$). To reduce the number of photo-stimulation parameters, all ensuing experiments used only 1 mW photo-stimuli.

Neural Activity Versus Hemodynamic Changes Evoked by Photo-stimulation and Forelimb Stimulation (Experiment 2)

Four-second forelimb or photo-stimulation trains were used to evoke changes in blood flow (LDF), blood volume (OIS–CBV) and blood oxygenation (OIS–BOLD) in the forelimb region of the somatosensory cortex. To inspect the spatial extent of the vascular response, OIS–CBV maps showing the temporal evolution of evoked forelimb and photo-stimulation responses were compared (Fig. 3A, top and middle row). Although the magnitude of the response (darkening) to photo-stimulation was larger and persisted for about 10 s longer, its spatial extent was similar to that from forelimb stimulation and suitable for further investigation. As a control, we previously examined the impact of photo-stimulation in a mouse model expressing GFP but lacking ChR2 using the same setup and found that no vascular responses were elicited when using the strongest photo-stimulation parameters (1 mW, 30 ms pulses; Fig. 3A, bottom row). The bright spot during the photo-stimulation period (blue circle in top-right corner of each frame) results from YFP excitation (or GFP in control mice) with the photo-stimulation laser light.

MUA and FP activity were recorded by electrophysiology at a single depth location (260 μm) to compare with the LDF and OIS data. As expected, forelimb stimulation evoked significant increases in spiking activity (Fig. 3B, bottom row). Photo-stimulation also evoked robust increases in MUA at this depth that scaled with photo-stimulus energy (Fig. 3B, top 3 rows). The average increase in MUA over prestimulation baseline was 2.4, 2.8, 1.8, and 1.0 spikes/s for forelimb stimulation and photo-stimulation with pulse durations of 30, 10, and 2 ms, respectively, though only comparisons against the shortest photo-stimulus (2 ms) response reached significance ($P < 0.05$, bar graph and error bars shown as default condition results in Fig. 4B). Interestingly, neural adaptation was observed during the photo-stimulation period, especially for the strongest photo-stimulus (30 ms in Fig. 3B). The ongoing spike rate decreased to near-zero following photo-stimulation for all parameters tested. FP activity, however, was not similar to MUA. Forelimb stimulation and photo-stimulation produced large increases in FP that waned during the stimulation period, but the FP activity was not modulated by the photo-stimulation

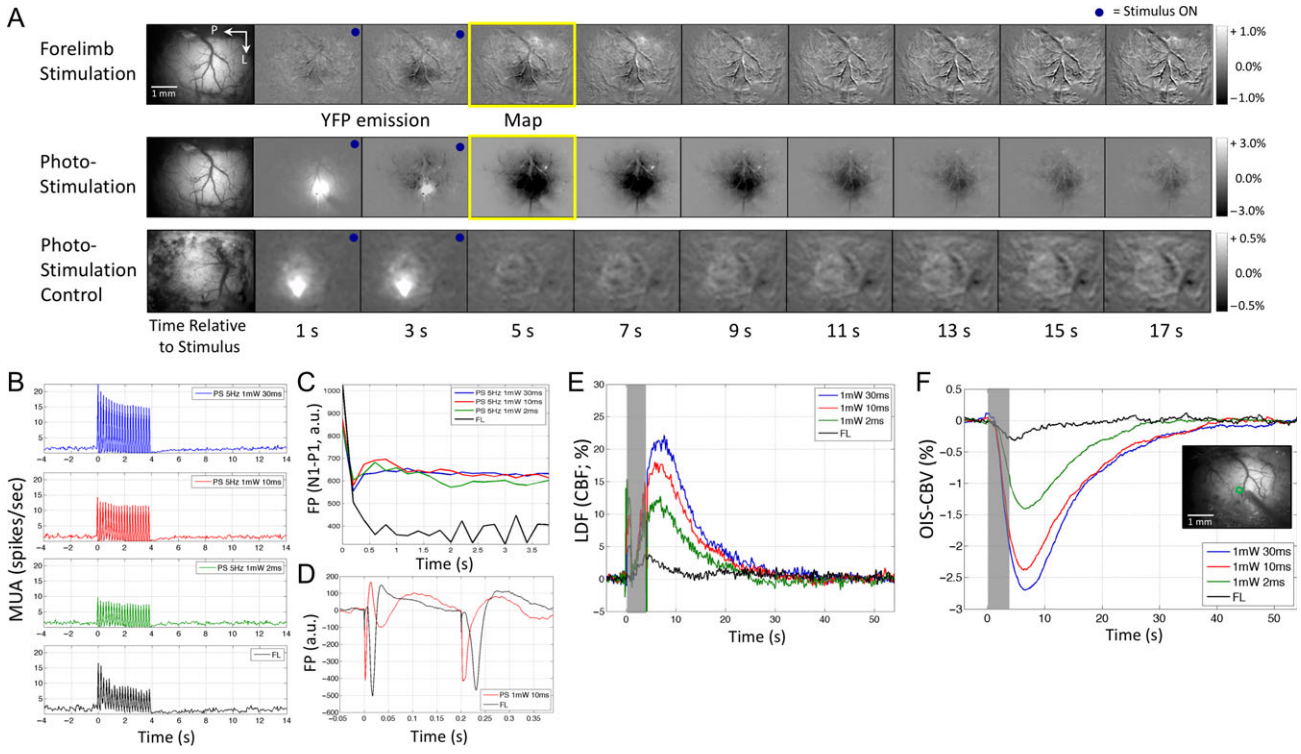

Figure 3. Neural and hemodynamic responses obtained under default conditions for Experiment 2. (*A*) Maps of the spatiotemporal evolution of hemodynamic responses (OIS–CBV) evoked by forelimb stimulation (top row) and photo-stimulation (10 ms pulse duration; middle row) in this mouse model (VGAT-ChR2). Maps from photo-stimulation of a control model (expressing GFP but not ChR2) are also shown (bottom row; 1 mW 30 ms pulses). The stimulation period lasted 4 s and is denoted by the blue dot on the top-right corner of each frame. Increases in blood volume absorb more light and are therefore manifested by darkening of the image. Photo-stimulation also excites YFP coexpressed with ChR2 in this mouse model (or GFP in the control model), hence, the brightened area showing the photo-stimulated location. (*B*) Average changes in multiunit activity (MUA) in response to photo-stimulation and forelimb stimulation (black line, bottom-most panel). (*C*) Average field potential (FP) response envelope during the stimulation period for both modes of stimulation. (*D*) Average FP trace showing the average changes in field potential of photo-stimulation (10 ms pulses, red line, top panel) and forelimb stimulation (black line, bottom panel). Small electrical stimulation artifacts are present for each delivered stimulus (5 Hz frequency or every 200 ms; first 2 pulses shown). (*E*) Average changes in cerebral blood flow (CBF) evoked by photo-stimulation or forelimb stimulation measured by laser Doppler flowmetry (LDF). The stimulation period is denoted by the gray bar. The rapid LDF increase with photo-stimulation onset is artefactual and due to interference between the LDF flowmeter and the photo-stimulation laser. (*F*) Average changes in OIS–CBV signal. Decreases in OIS–CBV correspond to increases in CBV. Inset shows a sample OIS–CBV image with the ROI location (green circle) for time series extraction.

energy (Fig. 3C). As a result, the average FP responses were not significantly different between these different stimulation parameters ($P > 0.20$; data not shown). This is likely the result of stimulating inhibitory neurons with no preferential directionality for synaptic currents (e.g., top-bottom). Inspection of the FP waveform shows typical N1-P1 peaks for forelimb stimulation as well as a small electrical stimulation artifact for each pulse delivered (Fig. 3D, bottom row). Photo-stimulation showed an initial complex multiphasic waveform that then turned biphasic for subsequent pulses (Fig. 3D) where the initial negative deflection peaked faster than that of forelimb evoked potentials.

Unlike the evoked neuronal activity, photo-stimulation generated relatively large hemodynamic responses compared with forelimb stimulation despite comparable levels of spiking activity (Fig. 3E,F). CBF increased with forelimb stimulation on average by 3.7 ± 1.6%, peaking 4.0 s after stimulation onset, and returned to baseline within 12 s after stimulation onset (Fig. 3E, black line). Photo-stimulation produced significantly larger increases in CBF compared with forelimb stimulation, which were effectively modulated by the photo-stimulus energy ($P < 0.01$ for all photo-stimulation parameters; Fig. 3E, blue–red–green lines). Average blood flow increases of 19.6%, 15.4%, and 11.0% with average time-to-peak of 6.5, 5.9, and 5.6 s, were measured for 30, 10, and 2 ms photo-stimulation pulses, respectively. Note that the photo-stimulus introduced artifacts into the LDF reading during the photo-stimulus duration, especially with stimulus onset. Although the responses to 30 and 10 ms were not significantly different, these were both significantly different to the responses evoked by 2 ms photo-stimuli ($P < 0.05$). As expected, the OIS–CBV responses were similar to the CBF responses measured by LDF and followed the same statistical significance results (Fig. 3F). OIS–BOLD responses were also acquired, those results are described in the Experiment 5 section below.

Neural Activity Versus Hemodynamic Changes Evoked Mostly by Stimulation of ChR2-Only Neurons (Experiment 3)

The same experiments were repeated after the administration of NMDA, AMPA, and kinate receptor antagonists (APV and NBQX) in a subset of animals. This glutamate receptor blockade was used to examine the electrophysiological and hemodynamic responses to activating inhibitory (VGAT-ChR2-positive) neurons, while suppressing the activation of excitatory neurons that may occur by disinhibition. The injected volume was estimated to be less than 0.1 μL based on spatial spread of the coinjected fluorescent label. After the intracortical administration of this pharmacological cocktail, spontaneous electrophysiological activity quieted immediately, indicative of its impact on cortical

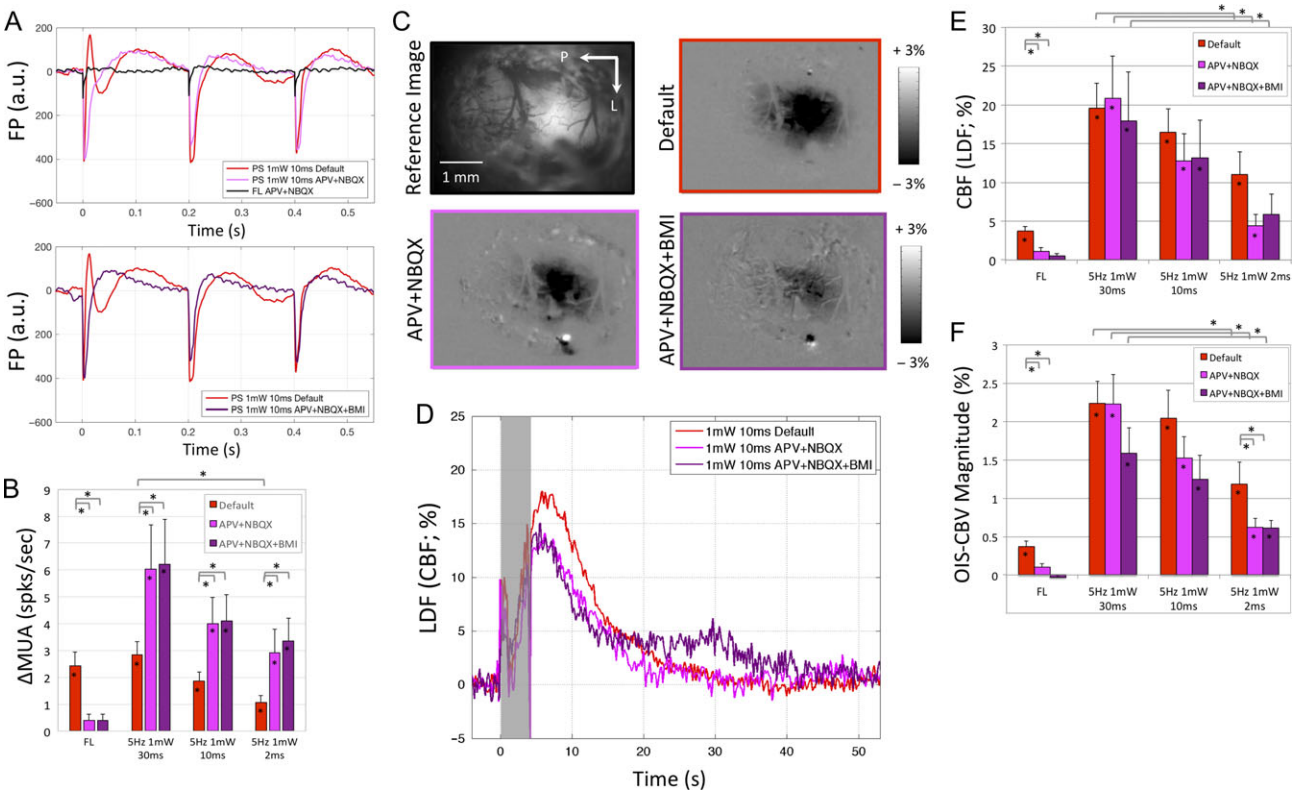

Figure 4. Neural and hemodynamic responses obtained under default (red), APV+NBQX (pink), and APV+NBQX+BMI (purple) conditions for Experiment 3. (*A*) Average field potential (FP) waveform for the first 3 forelimb (FL) and photo-stimulation pulses (10 ms pulse duration shown). (*B*) Average change in multiunit activity (ΔMUA) evoked by forelimb and photo-stimulation. (*C*) OIS–CBV maps obtained from a sample subject immediately after photo-stimulation under default (red border), APV + NBQX (pink border) and APV+NBQX+BMI conditions (purple border). Map scale bar is shown to the left of each row. (*D*) Average blood flow changes evoked by photo-stimulation (10 ms pulse duration shown) under the 3 conditions tested in Experiments 2 and 3. The gray bar denotes the photo-stimulation period. The initial rapid change with photo-stimulation onset and offset are artefactual and due to interference between the LDF flowmeter and photo-stimulus. Average change in CBF amplitude (*E*) and OIS–CBV magnitude (*F*) evoked by forelimb and photo-stimulation. Error bars denote standard error. Statistically significant differences ($P < 0.05$) are denoted by the asterisk in the bar (significantly greater than 0) or the lines above the bar graph for population comparisons. Significant comparisons between forelimb and photo-stimulation are not included in panels *B*, *E*, or *F* for visibility, most are significantly different, especially those from Experiment 2 and 3.

activity. As expected, forelimb stimulation did not produce significant FP or spiking activity under these pharmacological conditions (Fig. 4A,B). Surprisingly, the FP waveform changed from multiphasic to biphasic for all photo-stimulation pulses (Fig. 4A shows waveforms for 10 ms pulses). Following the first pulse in the stimulation period, the P1 peak occurred faster for the FP responses and the N1 width was slightly narrower. The addition of bicuculline (BMI) did not alter the FP responses further. The overall energy of the FP activity during the photo-stimulation period was significantly lower than that under default conditions ($P < 0.05$), on average by 25.5% and 32.5% after APV+NBQX and BMI administration, respectively. A general monotonic modulation of the FP amplitude was observed with photo-stimulation energy, with the 2 ms photo-stimulation FP amplitude significantly lower than those from 30 and 10 ms photo-stimulation ($P < 0.05$). The changes in the FP waveform suggest that photo-stimulation under default conditions engaged activity in a larger network of cells. Interestingly, the evoked increases in MUA were significantly larger under APV+NBQX and APV+NBQX+BMI than those measured under default conditions for all photo-stimulation parameters tested ($P < 0.05$, Fig. 4B).

Forelimb stimulation under these pharmacological conditions mostly abolished the evoked CBF and CBV responses (not significantly different from prestimulation baseline, $P > 0.1$), consistent with the electrophysiological findings above. The spatial extent of the hemodynamic responses generated by photo-stimulation were similar between conditions as seen in Figure 4C, although their magnitude were slightly lower. Average reductions for the photo-stimulation-evoked CBF responses of 25.5% and 25.1% were observed under APV+NBQX and APV+NBQX+BMI conditions compared with those under default conditions, respectively (Fig. 4D,E, reductions were only significant for 2 ms photo-stimulation). Similar results were observed for the OIS–CBV responses (Fig. 4F).

Neural Activity Versus Hemodynamic Responses Under NOS Blockade (Experiment 4)

To determine whether the hemodynamic responses evoked by photo-stimulation were mediated by nitric oxide, the same experiments were repeated in a different subset of animals under default conditions and after the intracortical administration of the NOS blocker L-NNA (Condition 3, Fig. 1B,D). No significant differences in the baseline blood flow level (+1.4 ± 7.3%) or the ongoing electrophysiological activity were detected before and after L-NNA administration ($P > 0.15$). In general, forelimb stimulation and photo-stimulation evoked FP waveforms that were somewhat similar preadministration and postadministration, but the amplitudes of the peaks differed and the width of the negative peak (N1) appeared to be slightly longer postagent administration. Overall, the FP amplitude tended to be lower after L-NNA administration while the evoked increases in MUA were not significantly different before and after agent administration ($P > 0.20$, Fig. 5A,B).

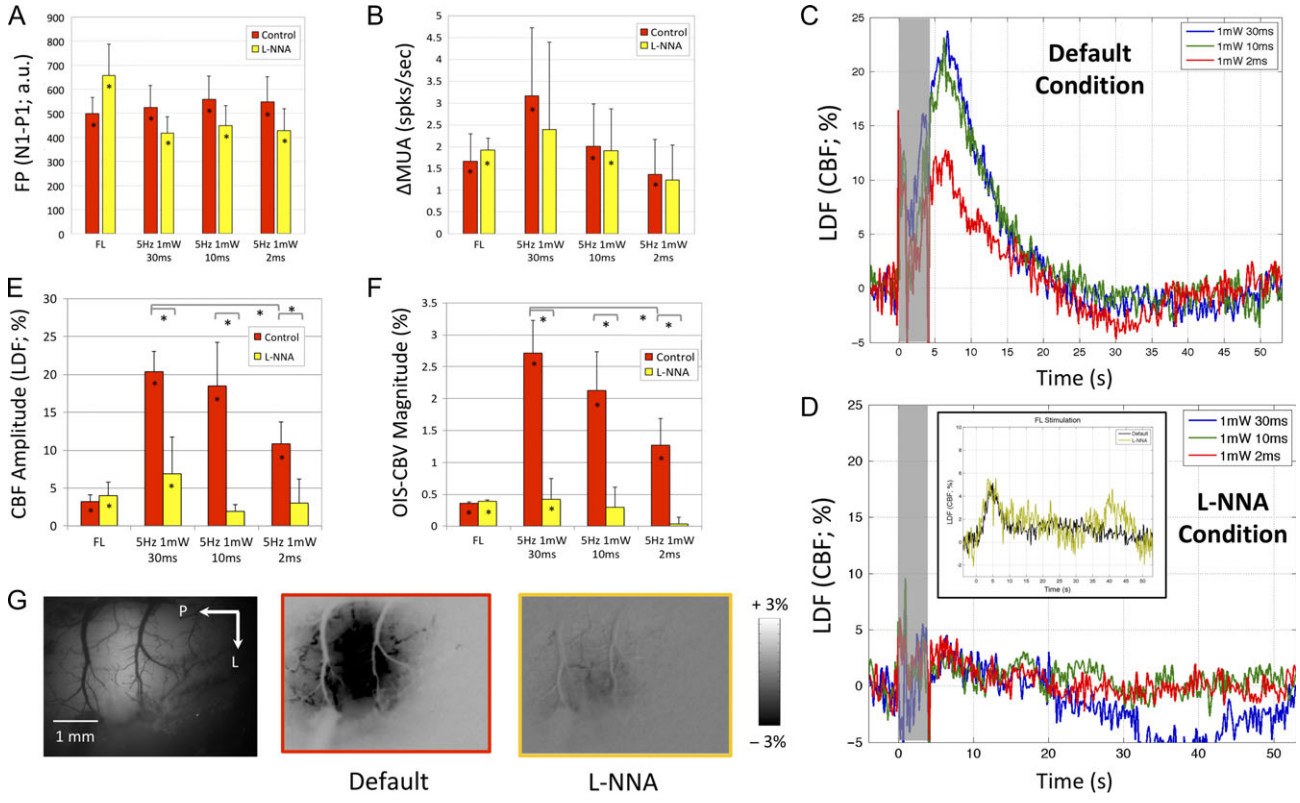

Figure 5. Neural and hemodynamic responses obtained under default and L-NNA conditions (Experiment 4). (*A*) Average field potential (FP) waveform evoked by photo-stimulation (10 ms pulse duration shown; top panel) and forelimb stimulation (bottom panel). (*B*) Average change in multiunit activity (ΔMUA), (*E*) CBF amplitude and (*F*) OIS–CBV magnitude for the different stimulation parameters. (*C*) Average changes in blood flow to the different photo-stimuli tested under default conditions and (*D*) after the intracortical administration of the NOS blocker L-NNA (0.5 mM). In general, small changes in blood flow were observed. The inset in *D* shows the changes in blood flow evoked by forelimb stimulation before and after L-NNA administration. (*G*) OIS–CBV maps produced by photo-stimulation (10 ms shown) in a sample subject. Error bars denote standard error. Statistically significant differences ($P < 0.05$) are denoted by the asterisk in the bar (significantly greater than 0) or the lines above the bar graph for population comparisons. Significant comparisons between forelimb and photo-stimulation are not included in panels *A*, *B*, *E*, or *F* to reduce clutter.

Forelimb stimulation produced similar LDF (CBF) and OIS–CBV responses preagent and postagent administration (Fig. 5D, inset, Fig. 5E,F). Similarly, photo-stimulation evoked responses under default conditions were indistinguishable from those obtained under default conditions for previous experiments (shown in Figs 3E,F and 5C). However, the changes in CBF and CBV evoked by photo-stimulation were significantly lower, with average reductions of 75.3 and 88.0%, respectively, after the administration of L-NNA ($P < 0.05$, Fig. 5C,D and E,F). Small residual increases were still observed that tended to correspond with the photo-stimulus energy for the OIS–CBV response but not for the LDF (CBF) response. The largest photo-stimulus also appeared to generate a poststimulus undershoot response that was observed in 2 of the animals tested. We inspected the OIS–CBV maps to check the spatial consistency of the hemodynamic response reduction and uniform changes were observed in most cases (Fig. 5G).

Differences in CMR_{O2} Between Excitatory and Inhibitory Optogenetic Models (Experiment 5)

For the last experimental group, the same setup and anesthesia conditions were used in Thy1-ChR2 mice, which target cortical excitatory neurons in Layer 5 (Wang et al. 2007). CBF, OIS–BOLD, and OIS–CBV responses to forelimb and photo-stimulation were recorded from both mouse models. Inspection of the spatial OIS–BOLD changes evoked by forelimb stimulation shows parenchymal decreases in the forelimb region followed by increases in OIS–BOLD signal especially in the venous vasculature (Fig. 6A, top panel). Photo-stimulation in Thy1-ChR2 mice showed changes in OIS–BOLD signal similar to those from forelimb stimulation (Fig. 6A, middle panel); however, photo-stimulation of VGAT-ChR2 mice showed large increases in OIS–BOLD signal in both tissue and venous locations without evident decreases in OIS–BOLD signal in the stimulated region (Fig. 6A, bottom panel). On average, simultaneously acquired LDF and OIS–BOLD responses from Thy1-ChR2 mice show moderate changes that scaled with the photo-stimulus duration (Fig. 6B,C; OIS–CBV responses shown in Fig. 3 of Vazquez et al. 2014). ROI-averaged OIS–BOLD responses (sample ROI shown in Fig. 1F) show evident negative changes of −0.06%, −0.13%, −0.11%, and −0.03% resulting from forelimb and 30, 10, and 2 ms photo-stimulation, respectively, that peaked near stimulation offset (all significantly greater than 0 with $P < 0.05$). Forelimb and photo-stimulation in VGAT-ChR2 mice evoked CBF responses that also scaled with the photo-stimulus duration (Fig. 6D); however, their OIS–BOLD

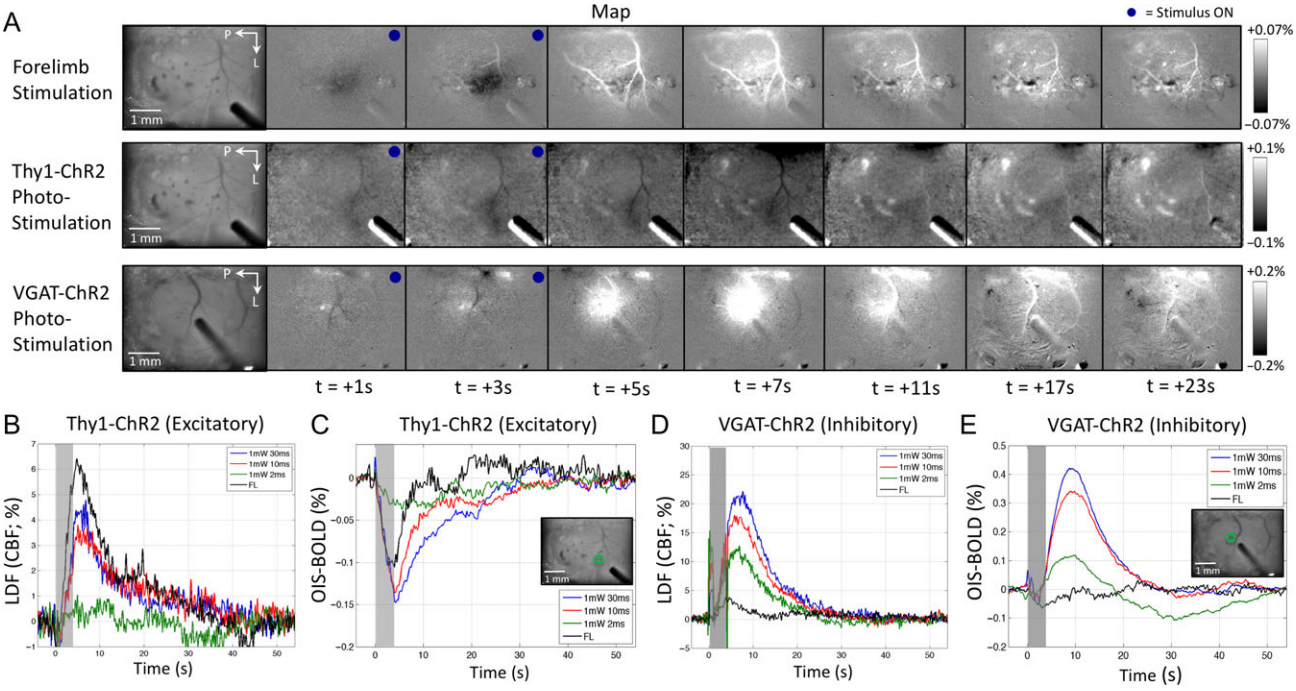

Figure 6. Changes in OIS–BOLD signal evoked by forelimb and photo-stimulation in excitatory and inhibitory optogenetic mouse models. (A) Example of spatiotemporal changes in OIS–BOLD signal in response to forelimb (FL, 5 Hz, top row panel) and photo-stimulation (PS) from one Thy1-ChR2 mouse (excitatory optogenetic model; middle row panel; 1 mW, 30 ms pulses at 5 Hz shown). Example of the spatiotemporal changes in OIS–BOLD signal evoked by photo-stimulation from one VGAT-ChR2 mouse (inhibitory optogenetic model; 1 mW, 10 ms pulses delivered at 5 Hz; bottom row panel). Each image sequence shows the baseline image on the left, followed by images of the changes in signal relative to baseline. Each frame shows the average change over a 1-s time span. The temporal sequence relative to stimulation onset is indicated below the bottom-most panel sequence in A. Evident decreases in OIS–BOLD signal are observed in parenchymal regions followed by increases especially in the venous vasculature and sinus to forelimb stimulation in Thy1-ChR2 mice. Mostly decreases in OIS–BOLD signal are observed in response to photo-stimulation of Thy1-ChR2 mice. On the other hand, large increases in OIS–BOLD signal are observed in parenchymal regions as well as venous vasculature as a result of photo-stimulation in VGAT-ChR2 mice. Decreasing the color scale extent did not reveal parenchymal decreases in OIS–BOLD signal in these mice. Average changes in blood flow and OIS–BOLD over the selected ROI (circular region centered on the insertion location of the electrode excluding surface vasculature) produced by forelimb and photo-stimulation from all Thy1-ChR2 mice (panels B and C, respectively) and all VGAT-ChR2 mice (panels D and E, respectively). Inset images in panels C and E show sample locations of the ROI (inner region inside the green circle). A sample ROI location is also presented in Figure 1F (green circle). The changes in blood flow and blood oxygenation evoked by forelimb stimulation were similar in both mouse models though slightly smaller in amplitude for the inhibitory mouse model. In the excitatory model, all changes in blood oxygenation were negative indicative of stimulation-evoked increases in tissue oxygen metabolism. However, the changes in blood oxygenation observed in inhibitory mice were large and positive, suggesting that the increases in blood flow were disproportionately larger to the increases in tissue oxygen metabolism.

responses were different from those evoked by forelimb stimulation (Fig. 6E). Photo-stimulation produced large OIS–BOLD responses that were mostly positive and peaked around 3–6 s after stimulation offset (Fig. 6E), while the forelimb OIS–BOLD responses were similar to those obtained in Thy1-ChR2 mice. Average increases in OIS–BOLD of +0.41%, +0.33%, and +0.11% were observed 7–10 s after stimulation onset in response to 30, 10, and 2 ms photo-stimulation, respectively. These results suggest that inhibitory neuron activity increased blood flow in disproportionate fashion to oxidative metabolism, at least compared with sensory activity, and that the increases in local blood oxygenation were mostly driven by the increases in blood flow. Decomposition of the OIS–CBV and OIS–BOLD data from excitatory and inhibitory mouse models to ΔHbO, ΔHbR, and ΔHbT agree with these observations (Supplementary Fig. S1). The changes in HbT largely resemble those obtained by OIS–CBV and the changes in HbR were similar to those obtained of OIS–BOLD (but opposite in polarity).

In the excitatory optogenetic model (Thy1-ChR2), changes in CMR_{O2} calculated from the ROI-averaged data yielded significant increases in oxygen metabolism of +2.0%, +1.5%, +1.2% following forelimb, 30 and 10 ms photo-stimulation, respectively (Fig. 7A,D). Although the shortest photo-stimulus (2 ms) did not appear to produce an evident increase in CMR_{O2} (or CBF), an average increase of 0.6% was calculated (significantly greater than 0 with $P < 0.05$). These results also indicate that the decreases in OIS–BOLD signal result from the increases in tissue CMR_{O2}. In VGAT-ChR2 mice, forelimb stimulation produced significant increases in CMR_{O2} of +2.9% ($P > 0.05$) while the changes in CMR_{O2} were not significantly different from 0 immediately following photo-stimulation ($P > 0.10$; Fig. 7B,E). However, prominent and significant decreases in oxygen metabolism of about −5% that peaked 9–14 s following the stimulation period were observed for 30 and 10-ms photo-stimuli ($P < 0.01$, Fig. 7B). Photo-stimulation for 2-ms showed a tendency towards an increase in CMR_{O2} following stimulation followed by a decrease (Fig. 7B, green line). Decreases in CMR_{O2} likely reflect the inhibition of excitatory activity and less so the metabolic load of inhibitory neuron activity, indicating that inhibitory neuron activity is not as metabolically demanding as excitatory

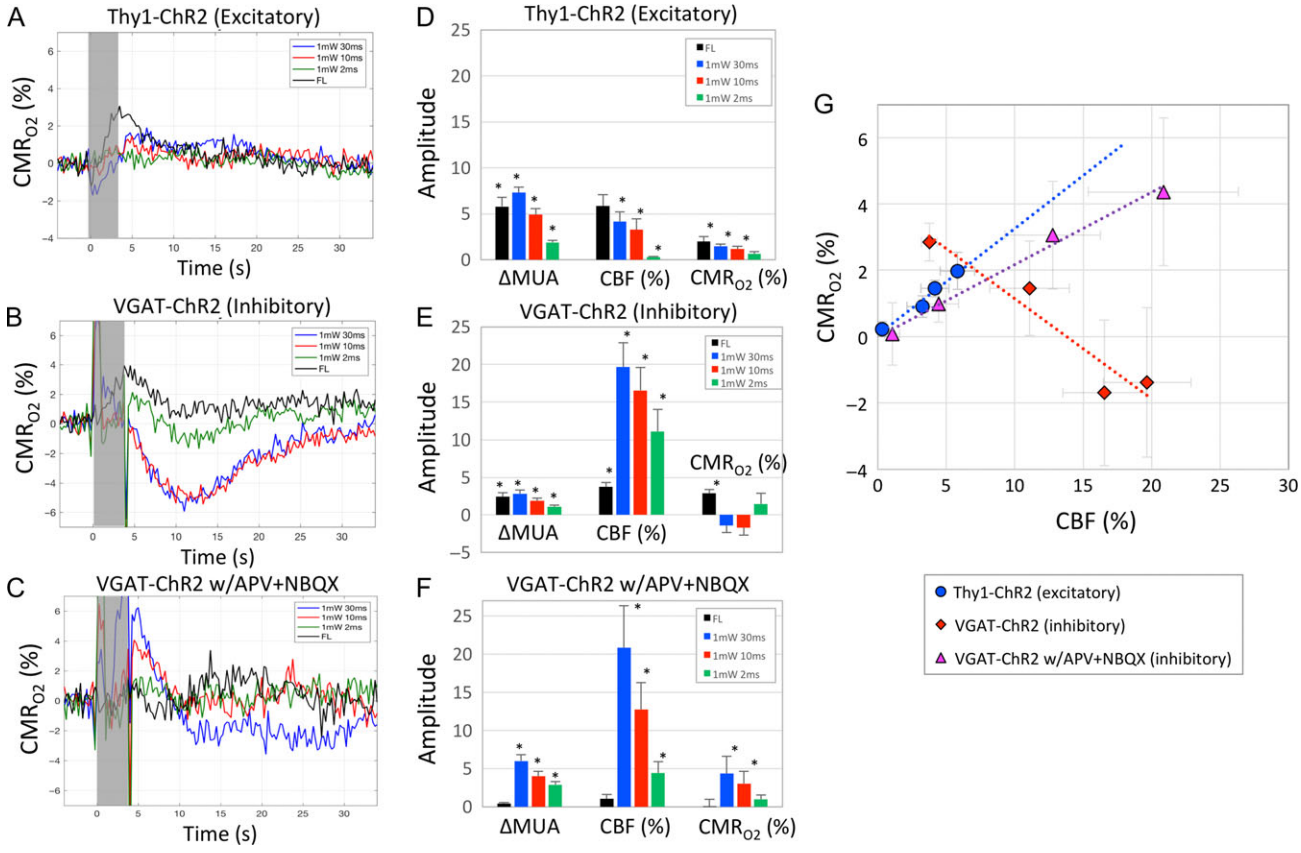

Figure 7. Estimates of CMR_{O2} changes evoked by forelimb and photo-stimulation in excitatory and inhibitory optogenetic mouse models. Average LDF, OIS–CBV and OIS–BOLD data from each animal were used to calculate changes in CMR_{O2} using Equation 1. Average changes in oxygen metabolism (CMR_{O2}; in % relative to baseline) due to forelimb and photo-stimulation are shown in (A) for Thy1-ChR2 mice (excitatory optogenetic mouse model) and (B) for VGAT-ChR2 mice (inhibitory optogenetic mouse model) under default conditions as well as (C) for VGAT-ChR2 mice under APV+NBQX conditions. The gray bar denotes the stimulation period; photo-stimulation introduced some artifacts into the data especially around stimulation onset and offset, hence, average time series during stimulation may not reflect actual changes (photo-stimulation data only). Summary bar graphs of the average changes in spiking activity (ΔMUA, spikes/s), changes in CBF (%) and changes in CMR_{O2} (%) are shown in panel D, panel E, and panel F for Thy1-ChR2 mice and VGAT-ChR2 mice under default conditions as well as VGAT-ChR2 mice under APV+NBQX conditions, respectively. The average spike rate was obtained during the stimulation period while the average change in CBF and CMR_{O2} was obtained as the average change between 4 and 7 s after stimulation onset for all animals. (G) Summary scatter plot of the average changes in CBF (%, x-axis) and CMR_{O2} (%, y-axis) from the excitatory mouse model (blue circles) and inhibitory mouse model (red diamonds for default condition responses and purple triangle for responses obtained under APV+NBQX conditions). A linear model was fit to all the data from each animal model and slopes of 0.321 ($P < 0.01$, $R^2 = 0.67$), −0.358 ($P > 0.15$, $R^2 = 0.04$) and 0.218 ($P < 0.01$, $R^2 = 0.53$) were calculated for the excitatory model and inhibitory model under default and APV+NBQX conditions, respectively. Error bars denote standard error. All 3 linear models were significantly different from one another ($P > 0.10$). Statistically significant differences are denoted by the asterisk in the bar (significantly different from 0, $P < 0.05$).

neuron activity. To explore this further, under the glutamate receptor blockade (APV and NBQX), excitatory neuron activity is not modulated before, during, or after photo-stimulation. Under this pharmacological condition, we calculated that inhibitory neuron activity increases CMR_{O2} in proportion to the evoked activity (Fig. 7C,F). The increases in CMR_{O2} were significantly different from 0 for the responses evoked by 30 and 10 ms photo-stimuli ($P < 0.05$). Note that the baseline metabolic rate is likely to be significantly lower under this condition, preventing a direct comparison between conditions. Absolute (not relative) changes in CMR_{O2} would be necessary for further metabolic load comparisons between these conditions.

In summary, photo-stimulation evoked CBF and CMR_{O2} responses were positively modulated by spiking activity in Thy1-ChR2 mice (excitatory optogenetic model; Fig. 7G). A linear fit yielded a significant relationship between CBF and CMR_{O2} amplitudes with slope of 0.321 (Fig. 7G). Photo-stimulation evoked a much larger CBF response in VGAT-ChR2 mice (inhibitory optogenetic model) compared with CMR_{O2} responses, even under APV+NBQX conditions (Fig. 7E,F). A linear fit of the CBF and CMR_{O2} amplitude data under APV+NBQX conditions yielded a significant relationship with slope of 0.218 (Fig. 7G). Further, these 2 linear models were significantly different with $P > 0.10$, indicating a mismatch of 47%.

Discussion

This work examined the contribution of inhibitory neuron activity on hemodynamic responses captured by changes in blood flow, blood volume, and blood oxygenation in the cortex of lightly anesthetized mice. These data were obtained under 3 different pharmacological conditions to reduce potential contributions from postsynaptic activity, excitatory or inhibitory, on hemodynamic responses and also investigate the role of nitric oxide in the generation of inhibitory activity-driven increases in blood flow. Because cortical activity is not commonly initiated by inhibitory neurons, experiments were initially conducted to examine the neuronal activity properties elicited by photo-stimulation. The photo-stimulation parameters selected evoked graded levels of activity throughout the cortical depth and did not exceed that of sensory forelimb stimulation. We observed comparable increases in neuronal activity evoked by forelimb and photo-stimulation; however, significantly larger increases in blood flow and volume were produced by photo-stimulation of inhibitory neurons compared with forelimb stimulation. These hemodynamic changes are in agreement with previous reports (Anenberg et al. 2015; Uhlirova et al. 2016). Following blockade of glutamate and $GABA_A$ receptors, slight changes in the FP waveform were observed but neuronal activity was still reliably modulated by photo-stimulation. Under these conditions, hemodynamic changes persisted, though slightly reduced. More importantly, photo-stimulation-evoked changes in blood flow and blood volume were suppressed by 75–80% with the administration of L-NNA, a nitric oxide synthase inhibitor, suggesting that inhibitory neurons mostly regulate blood flow via nitric oxide. Lastly, eliciting initial excitatory neuron activity by optogenetics in Thy1-ChR2 mice or forelimb stimulation in VGAT-ChR2 mice produced local decreases in blood oxygenation. On the other hand, large increases in blood oxygenation were consistently produced by optogenetic stimulation of inhibitory neurons in VGAT-ChR2 mice. CMR_{O2} calculations showed that although inhibitory neuron activity elicits increases in tissue oxygen consumption, their contribution to the overall tissue metabolic load under normal conditions is small, at least compared with excitatory neuron activity. These results indicate a mismatch between the metabolic rate and blood flow regulation properties of inhibitory and excitatory neurons.

Our initial experiments aimed to ensure photo-stimulation evoked activity throughout the cortex. This is an important criterion because different types of inhibitory neurons are known to exist at preferable depths. For example, Chandelier-type neurons tend to concentrate in Layers 2 and 6 while NPY-expressing neurons are more uniformly distributed between Layers 2 and 6 (Taniguchi et al. 2013; Taniguchi 2014). The weakest photo-stimulation parameter (1 mW, 2 ms pulses) evoked small amounts of activity in deep cortical locations. It is worth noting that spikes evoked in the superficial layers occurred about 4 ms sooner than spikes in deeper layers. It is possible that this systematic bias has an impact on the evoked activity; however, evident differences in activity patterns with depth were not observed. The other criterion used to select photo-stimulation parameters was that the evoked activity did not exceed that of forelimb-evoked activity at any depth. The rationale being that photo-stimulation might induce large amounts of spiking activity above normal physiological limits. In this regard, sensory forelimb stimulation is a generous upper bound when using MUA as a metric since it evokes activity from excitatory and inhibitory neurons. The strongest photo-stimulation parameter set selected evoked relatively large amounts of activity that neared that of forelimb at many depths. Nonetheless, these parameters were deemed suitable and were used for further experimentation.

Under default conditions (light ketamine anesthesia), repeated stimulation trains were delivered to elicit robust hemodynamic responses. Photo-stimulation evoked robust spiking activity in layers 2–3 that was similar to forelimb stimulation; that is, 30-ms photo-stimulation pulses evoked MUA slightly larger than forelimb stimulation, while 10-ms pulses evoked MUA slightly lower. Neural adaptation was observed in both forelimb and photo-stimulation, but it was more pronounced for stronger photo-stimuli. Interestingly, Anenberg et al. (2015) used a glass electrode to measure spiking activity in deeper cortical locations (400–550 μm) and observed typical inhibitory effects where spiking activity was suppressed during photo-stimulation. It is likely that their glass electrode's spatial sensitivity is more confined than our carbon fiber electrode. We did observe suppression of spiking activity between pulses and also for a few seconds following photo-stimulation which was also observed by Anenberg. Our blood flow responses evoked by photo-stimulation were similar to those obtained by Anenberg, although the stimulation parameters were different. Anenberg's photo-stimulus lasted 1-s (5 ms 2 mW pulses at 100 Hz) and elicited blood flow responses around +20%, while our strongest photo-stimulus also produced increases in blood flow around 20% though to a longer stimulus duration (4 s). Differences in amplitude are likely due to our lower photo-stimulus intensity (1 mW). The temporal shape of the blood flow responses were also similar, both showing prominent increases in blood flow that peaked shortly after stimulus cessation (0.5–2.5 s). Uhlrilova et al. (2016) reported prominent increases in vessel (arterial) diameter of about +8% (measured by two-photon microscopy under alpha-chloralose anesthesia) that peaked around 1–2 s after stimulus offset depending on the depth of the measurements. Inspection of our OIS–CBV maps also show strong pial arterial dilations. Poststimulation decreases in blood flow responses were not generally observed in our data or Anenberg's data; however, Uhlirova showed

consistent decreases in blood flow following prominent increases, especially deeper in the cortex. The responses we measured are biased towards the surface, hence it is possible that poststimulation decreases occur but are not detectable by our measurements. Although the temporal shape of forelimb stimulation evoked hemodynamic responses was similar to that evoked by photo-stimulation, the forelimb response time-to-peak was faster, occurring at the end of the stimulation period. However, one of the biggest differences in our findings is the large difference between forelimb and photo-stimulation evoked responses (about 65–80% lower). This finding suggests that inhibitory neurons can have a significant impact on local blood flow regulation as shown in slice experiments (Cauli 2004). This notion is supported by findings from Anenberg et al. and Uhrilova et al. though not as striking since optogenetic stimulation produced hemodynamic changes that were larger than sensory stimulation but closer in amplitude.

The cortical circuit depicted in Figure 1 serves as a simplified operational circuit for the pharmacological experiments performed. To prevent stimulation-evoked activity from propagating throughout the connected network, glutamate receptor antagonists (APV and NBQX) were used to block excitatory postsynaptic activity. Recent studies have found that inhibitory neuron activity can dampen excitatory activity, and also increase excitatory activity via inhibitory-to-inhibitory neuron connections that disinhibit excitatory neurons (Pfeffer et al. 2013; Pi et al. 2013). Therefore, photo-stimulation of inhibitory neurons under the glutamate receptor blockade will partly restrict activity to ChR2-expressing neurons. To further restrict inhibitory neuron activity, a $GABA_A$ receptor antagonist (BMI) was also used. Our results show robust hemodynamic responses under these conditions that were somewhat reduced relative to the default condition. Similar results were obtained by Anenberg using a similar pharmacological blockade. However, Uhlirova showed that blockade of sodium channels with TTX effectively abolished photo-stimulation evoked hemodynamic responses. These results suggest that the reductions in blood flow responses are probably due to neurovascular mechanisms downstream from inhibitory neuron activity, such as disinhibition of excitatory neuron activity. Our neural recordings show changes in the FP waveform under these pharmacological conditions. Interestingly, the photo-stimulation evoked increases in spiking activity were larger compared with those under default conditions. Inspection of the raw data suggests that this was due to a shift from complex spike waveforms to simpler spike waveforms under these conditions. Altogether, these results show that inhibitory neurons can effectively regulate local blood flow in cortex and appear to do so more effectively than excitatory neuron activity (at least evoked by sensory stimulation).

We also sought to determine whether nitric oxide plays a significant role in the generation of blood flow responses evoked by inhibitory neuron activity. Nitric oxide is a freely diffusible molecule that is generated by nitric oxide synthase activity in endothelial cells and subpopulations of inhibitory neurons. Upregulation of NOS activity is associated with NMDA receptor activity and calcium influx (Christopherson et al. 1999). Nitric oxide stimulates the production of cGMP leading to the smooth muscle cell relaxation. Previous studies have investigated the role of nitric oxide on sensory-evoked hemodynamic responses, which is primarily evoked by excitatory neuron activity. In rodents, the application of NOS blockers, such as L-NNA or L-NAME, had either no effect or moderate effect at reducing sensory-evoked blood flow responses (Adachi et al. 1994; Yang et al. 1998; Lindauer et al. 1999; Lauritzen 2001; Nielsen and Lauritzen 2001; Matsuura and Kanno 2002; Shibuki et al. 2004; Kitaura et al. 2007; Li et al. 2011). In these studies, complete or near-complete mitigation of blood flow responses was not achieved, with more consistent agreement over slight reductions in sensory evoked blood flow responses. In our studies, we observed no evident reduction of sensory-evoked responses after the application of L-NNA. This was unexpected since L-NNA is commonly used for general blockade of NOS enzyme activity, including that of endothelial NOS. Perhaps intracortical application of this agent avoided effects at the level of pial vasculature (most studies apply them topically or intravenous) and/or endothelial cells that might work to attenuate sensory evoked responses. The baseline blood flow level was not significantly different after L-NNA administration (+1.4 ± 7.3%). Another possibility is that the forelimb stimulus did not recruit significant activity from inhibitory neurons that strongly regulate blood flow (e.g., NO-releasing inhibitory neurons) under light ketamine anesthesia. It is also possible that the slightly larger evoked increase in forelimb-evoked spiking activity (though not statistically significant) may account for the similarity in hemodynamic response amplitude. More importantly, local delivery of L-NNA significantly reduced photo-stimulation evoked increases in blood flow although neural activity was not significantly altered. This clear suppression indicates that inhibitory neurons largely regulate local blood supply via nitric oxide release, which is likely stimulated by a photo-stimulation-evoked influx in calcium in NOS-expressing inhibitory neurons. Residual increases in blood flow may be due to an incomplete NOS blockade or the involvement of other neurovascular signaling pathways (e.g., GABA, adenosine, or prostaglandins) (Cauli and Hamel 2010).

Our last experiment sought to compare differences in oxygen metabolism between excitatory and inhibitory neuron activity. The tissue ROI used excluded larger surface vasculature to ensure sensitivity to the local tissue changes. Upon inspection of the data, it is evident that changes in blood oxygenation evoked by sensory and photo-stimulation in Thy1-ChR2 mice (excitatory optogenetic model) show comparable increases in tissue oxygen consumption relative to blood flow. In agreement with this notion, the calculated CMR_{O2} changes show increases that persist following stimulation offset. The average CBF-to-CMR_{O2} ratio for photo-stimulation responses in this model is 2.6 (average ratio excluding forelimb data). Decomposed reduced-hemglobin (HbR) time series show increases with similar temporal profile as OIS–BOLD (Supplementary Fig. S1). Hence, the decreases in OIS–BOLD from Thy1 mice are deduced to stem from the increases in tissue CMR_{O2} in the presence of modest but not large CBF increases. On the other hand, photo-stimulation of VGAT-ChR2 mice (inhibitory optogenetic model) produced prominent increases in blood oxygenation, suggesting a disproportionately larger increase in blood flow relative to parenchymal oxygen consumption. Decomposed reduced-hemglobin (HbR) time series also show similar temporal profiles to OIS–BOLD (Supplementary Fig. S1). The calculated CMR_{O2} changes were not similar to the forelimb response; instead, it showed a slower and prominent decrease that likely reflects decreases in excitatory neuron activity. If inhibitory neuron activity increases oxygen consumption, it is either small or overwhelmed by reductions in excitatory neuron metabolism. If this notion is correct, it is interesting that poststimulation reductions in blood flow due to reduced excitatory neuron activity were not observed, although decreases in MUA following optogenetic stimulation were present. Similarly, the decrease in oxygen consumption suggests

that disinhibition of excitatory neurons was not prominent enough to produce an evident increase in CMR_{O2}. The calculated changes in CMR_{O2} under the glutamate receptor blockade showed only increases in oxygen metabolism with photo-stimulation, supporting the notion of decreased excitatory activity as a result of inhibitory activity under default conditions. Because the baseline oxygen consumption rates are likely different between default and APV+NBQX conditions, we cannot directly compare the changes in oxygen consumption evoked by photo-stimulation under these conditions. However, the average CBF-to-CMR_{O2} ratio under this condition for optogenetic responses was 4.5, suggesting that the CBF-to-CMR_{O2} mismatch between excitatory and inhibitory neurons is at least 47% (4.5:2.6 = 73%). Our findings are consistent with reports that synaptic activity is metabolically expensive and given that excitatory neurons outnumber inhibitory neurons in cortex, excitatory neuron activity would more closely track the tissue metabolic rate. Similar metabolic findings were generally observed in magnetic resonance spectroscopy (MRS) studies in the absence of evoked stimulation, where the glucose oxidation directed to excitatory neurons was about 5× larger than that directed to GABA neurons (Patel et al. 2005; Duarte and Gruetter 2013).

There are several possible sources of error for our CMR_{O2} calculations. First, resting hemoglobin concentration and oxygen saturation levels were assumed based on literature values. Although the levels chosen are reasonable for our experimental conditions, the calculated changes depend on these values. While it is possible to calibrate our measurements to changes in oxygen consumption using a blood flow stimulus (e.g., hypercapnia stimulation), this approach also requires additional assumptions. Second, the model we chose assumes steady-state conditions, such that oxygen delivered to tissue is immediately consumed. This assumption influences the temporal shape of the calculated CMR_{O2} changes, but not likely by a significant amount considering that oxygen is metabolized relatively fast (Vazquez et al. 2012).

We do not discard the possibility that light-ketamine anesthesia might alter cortical excitability of excitatory and inhibitory neurons or the engagement of neurovascular pathways. For our previous study, our choice of experimental anesthesia was based on observations that robust neural and hemodynamic responses are maintained under light ketamine anesthesia and that it did not significantly alter basal vascular tone. Our motivation to use this anesthesia for this study was to more directly compare hemodynamic responses obtained from excitatory and inhibitory optogenetic mouse models as well as its necessity to perform more invasive electrophysiological recordings and pharmacologically modulate cortical physiology. The hemodynamic responses obtained in this study were smaller than those obtained from our group in anesthetized rats, but they were statistically significant and in correspondence with the evoked spiking activity (Figs 3, 4, 7 and Supplementary Fig. S2). In contrast, Uhlirova et al. (2016) performed experiments in alpha-chloralose-anesthetized mice as well as awake (head-fixed) mice and showed that the hemodynamic response was similar between these two conditions. Nonetheless, comparison of the blood flow and blood volume responses from excitatory and inhibitory mouse models under the same experimental conditions show similar response shapes but differences in amplitude, consistent with the notion that inhibitory neurons play a significant role in cortical blood flow regulation in proportion to their activity. It is possible that differences in temporal shape could be used to differentiate excitatory and inhibitory activity patterns from hemodynamic responses, but additional experimental data is necessary to determine its feasibility. Lastly, inhibitory neuron dysfunction will likely have an impact on the amplitude and shape of the hemodynamic responses.

Implications

Our findings indicate that inhibitory neuron activity, although it effectively suppresses excitatory neuron activity, is capable of producing significant increases in blood flow and hemodynamic responses (Supplementary Fig. S2). Therefore, reductions in blood flow and blood oxygenation are likely the result of decreases in neuronal activity and less likely the result of inhibitory neuron activity. However, the mouse model used in this study targets most (if not all) GABA neurons in cortex, and it is likely that only subpopulations of GABA neurons (in particular NO releasing neurons) contribute to increases in blood flow, while other subpopulations may reduce it (e.g., poststimulation undershoot reported by Uhrilova). In addition, inhibitory activity blood flow responses were not completely abolished by NOS blockade, it is possible that other pathways such as cyclooxygenase-2 (COX-2) and prostaglandings (PGE2), which are thought to be principal pathways of neurovascular regulation from excitatory neurons, contribute to blood flow regulation from inhibitory neurons. Additional studies are necessary to determine the contribution of different subtypes of GABA neurons on blood flow regulation.

Supplementary Material

Supplementary material is available at *Cerebral Cortex* online.

Funding

National Institutes of Health (NIH) grants (R01-NS094404 to A. V.) and (R01-EB003324 to M.F.), a MNIRG grant from the Alzheimer's Association (A.V.) and a grant from the Institute for Basic Science (Korea) (IBS-R15-D1 to S.G.K.).

Notes

Conflict of Interest: None declared.

References

Adachi K, Takahashi S, Melzer P, Campos KL, Nelson T, Kennedy C, Sokoloff L. 1994. Increases in local cerebral blood flow associated with somatosensory activation are not mediated by NO. Am J Physiol. 267:H2155–H2162.

Altamura C, Dell'Acqua ML, Moessner R, Murphy DL, Lesch KP, Persico AM. 2007. Altered neocortical cell density and layer thickness in serotonin transporter knockout mice: a quantitation study. Cereb Cortex. 17:1394–1401.

Anenberg E, Chan AW, Xie Y, LeDue JM, Murphy TH. 2015. Optogenetic stimulation of GABA neurons can decrease local neuronal activity while increasing cortical blood flow. J Cereb Blood Flow Metab. 35:1579–1586.

Armstrong-James M, Fox K, Das-Gupta A. 1992. Flow of excitation within rat barrel cortex on striking a single vibrissa. J Neurophysiol. 68:1345–1358.

Boorman L, Harris S, Bruyns-Haylett M, Kennerley A, Zheng Y, Martin C, Jones M, Redgrave P, Berwick J. 2015. Long-latency reductions in gamma power predict hemodynamic changes that underlie the negative BOLD signal. J Neurosci. 35: 4641–4656.

Buxton RB, Wong EC, Frank LR. 1998. Dynamics of blood flow and oxygenation changes during brain activation: the balloon model. Magn Reson Med. 39:855–864.

Cauli B. 2004. Cortical GABA interneurons in neurovascular coupling: relays for subcortical vasoactive pathways. J Neurosci. 24:8940–8949.

Cauli B, Hamel E. 2010. Revisiting the role of neurons in neurovascular coupling. Front Neuroenergetics. 2:9.

Christopherson KS, Hillier BJ, Lim WA, Bredt DS. 1999. PSD-95 assembles a ternary complex with the N-methyl-D-aspartic acid receptor and a bivalent neuronal NO synthase PDZ domain. J Biolog Chem. 274:27467–27473.

Davis T, Kwong K, Weisskoff R, Rosen B. 1998. Calibrated functional MRI: mapping the dynamics of oxidative metabolism. Proc Natl Acad Sci USA. 95:1834–1839.

Devor A, Hillman EMC, Tian P, Waeber C, Teng IC, Ruvinskaya L, Shalinsky MH, Zhu H, Haslinger RH, Narayanan SN, et al. 2008. Stimulus-induced changes in blood flow and 2-deoxyglucose uptake dissociate in ipsilateral somatosensory cortex. J Neurosci. 28:14347–14357.

Duarte JMN, Gruetter R. 2013. Glutamatergic and GABAergic energy metabolism measured in the rat brain by (13) C NMR spectroscopy at 14.1 T. J Neurochem. 126:579–590.

Dunn AK, Devor A, Dale AM, Boas DA. 2005. Spatial extent of oxygen metabolism and hemodynamic changes during functional activation of the rat somatosensory cortex. Neuroimage. 27:279–290.

Hillman EMC. 2014. Coupling mechanism and significance of the BOLD signal: a status report. Annu Rev Neurosci. 37:161–181.

Horecker BL. 1943. The absorption spectra of hemoglobin and its derivatives in the visible and near infra-red regions. J Biolog Chem. 148:173–183.

Jones M, Berwick J, Johnston D, Mayhew J. 2001. Concurrent optical imaging spectroscopy and laser-Doppler flowmetry: the relationship between blood flow, oxygenation, and volume in rodent barrel cortex. Neuroimage. 13:1002–1015.

Kida I, Hyder F. 2006. Physiology of functional magnetic resonance imaging: energetics and function. Methods Mol Med. 124:175–195.

Kim SG, Rostrup E, Larsson HB, Ogawa S, Paulson OB. 1999. Determination of relative CMRO2 from CBF and BOLD changes: significant increase of oxygen consumption rate during visual stimulation. Magn Reson Med. 41:1152–1161.

Kitaura H, Uozumi N, Tohmi M, Yamazaki M, Sakimura K, Kudoh M, Shimizu T, Shibuki K. 2007. Roles of nitric oxide as a vasodilator in neurovascular coupling of mouse somatosensory cortex. Neurosci Res. 59:160–171.

Lauritzen M. 2001. Relationship of spikes, synaptic activity, and local changes of cerebral blood flow. J Cereb Blood Flow Metab. 21:1367–1383.

Lewis DA, Hashimoto T, Volk DW. 2005. Cortical inhibitory neurons and schizophrenia. Nat Rev Neurosci. 6:312–324.

Li J, Bravo DS, Upton AL, Gilmour G, Tricklebank MD, Fillenz M, Martin C, Lowry JP, Bannerman DM, McHugh SB. 2011. Close temporal coupling of neuronal activity and tissue oxygen responses in rodent whisker barrel cortex. Eur J Neurosci. 34:1983–1996.

Lindauer U, Megow D, Matsuda H, Dirnagl U. 1999. Nitric oxide: a modulator, but not a mediator, of neurovascular coupling in rat somatosensory cortex. Am J Physiol. 277:H799–H811.

Matsuura T, Kanno I. 2002. Effect of nitric oxide synthase inhibitor on the local cerebral blood flow evoked by rat somatosensory stimulation under hyperoxia. Comp Biochem Physiol A Mol Integr Physiol. 131:267–274.

Nielsen AN, Lauritzen M. 2001. Coupling and uncoupling of activity-dependent increases of neuronal activity and blood flow in rat somatosensory cortex. J Physiol. 533:773–785.

Patel AB, de Graaf RA, Mason GF, Rothman DL, Shulman RG, Behar KL. 2005. The contribution of GABA to glutamate/glutamine cycling and energy metabolism in the rat cortex in vivo. Proc Natl Acad Sci USA. 102:5588–5593.

Perrenoud Q, Rossier J, Férézou I, Geoffroy H, Gallopin T, Vitalis T, Rancillac A. 2012. Activation of cortical 5-HT(3) receptor-expressing interneurons induces NO mediated vasodilatations and NPY mediated vasoconstrictions. Front Neural Circuits. 6:50.

Pfeffer CK, Xue M, He M, Huang ZJ, Scanziani M. 2013. Inhibition of inhibition in visual cortex: the logic of connections between molecularly distinct interneurons. Nat Neurosci. 16:1068–1076.

Pi H-J, Hangya B, Kvitsiani D, Sanders JI, Huang ZJ, Kepecs A. 2013. Cortical interneurons that specialize in disinhibitory control. Nature. 503:521–524.

Shibuki K, Hishida R, Murakami H, Kudoh M, Kawaguchi T, Watanabe M, Watanabe S, Kouuchi T, Tanaka R. 2004. Dynamic imaging of somatosensory cortical activity in the rat visualized by flavoprotein autofluorescence. J Physiol. 549:919–927.

Shmuel A, Augath M, Oeltermann A, Logothetis NK. 2006. Negative functional MRI response correlates with decreases in neuronal activity in monkey visual area V1. Nat Neurosci. 9:569–577.

Sloviter RS. 1987. Decreased hippocampal inhibition and a selective loss of interneurons in experimental epilepsy. Science. 235:73–76.

Stefanovic B, Warnking JM, Pike GB. 2004. Hemodynamic and metabolic responses to neuronal inhibition. Neuroimage. 22: 771–778.

Taniguchi H. 2014. Genetic dissection of GABAergic neural circuits in mouse neocortex. Front Cell Neurosci. 8:1–22.

Taniguchi H, Lu J, Huang ZJ. 2013. The spatial and temporal origin of chandelier cells in mouse neocortex. Science. 339:70–74.

Uhlirova H, Kılıç K, Tian P, Thunemann M, Desjardins M, Saisan PA, Sakadžić S, Ness TV, Mateo C, Cheng Q, et al. 2016. Cell type specificity of neurovascular coupling in cerebral cortex. eLife. 5: e14315. doi: 10.7554/eLife.14315

Vazquez AL, Fukuda M, Crowley JC, Kim S-G. 2014. Neural and hemodynamic responses elicited by forelimb- and photostimulation in channelrhodopsin-2 mice: insights into the hemodynamic point spread function. Cereb Cortex. 24: 2908–2919.

Vazquez AL, Fukuda M, Kim S-G. 2012. Evolution of the dynamic changes in functional cerebral oxidative metabolism from tissue mitochondria to blood oxygen. J Cereb Blood Flow Metab. 32:745–758.

Wang H, Peca J, Matsuzaki M, Matsuzaki K, Noguchi J, Qiu L, Wang D, Zhang F, Boyden E, Deisseroth K, et al. 2007. High-speed mapping of synaptic connectivity using photostimulation in Channelrhodopsin-2 transgenic mice. Proc Natl Acad Sci USA. 104:8143–8148.

Yang G, Feddersen R, Zhang F, Clark H, Beitz A, Iadecola C. 1998. Cerebellar vascular and synaptic responses in normal mice and in transgenics with Purkinje cell dysfunction. Am J Physiol. 274:R529–R540.

Zhao S, Ting JT, Atallah HE, Qiu L, Tan J, Gloss B, Augustine GJ, Deisseroth K, Luo M, Graybiel AM, et al. 2011. Cell type–specific channelrhodopsin-2 transgenic mice for optogenetic dissection of neural circuitry function. Nat Methods. 8: 745–752.